Biped Humanoid Robot Mahru III

Woong Kwon, Hyun K. Kim, Joong Kyung Park, Chang Hyun Roh,
Jawoo Lee, Jaeho Park, Won-Kuk Kim, and Kyungshik Roh
Mechatronics & Manufacturing Technology Center,
Samsung Electronics Co., Ltd.
Suwon-Shi, Kyunggi-Do, 443-742, Republic of Korea
Email: wkwon@samsung.com

***Abstract*— This paper presents a new biped humanoid robot Mahru III (150cm, 62Kg) developed by Samsung Electronics Co., Ltd in 2007. The ultimate goal of this project is to design biped humanoid robots connected to a wireless network environment so that they can be used in our daily life. As the first step, Mahru III was built as a pilot platform for future household companion robots. In this paper we focus on the design of the mechanical system, electrical/electronic parts, and the control algorithm with some experimental results. We designed the mechanical system to achieve lightweight, high stiffness and high energy efficiency through CAE(Computer Aided Engineering) analysis and DOE(Design of Experiments)-based optimization. We also built an extensible electrical/electronic system to provide for future network-based applications. Walking control algorithm is realized to make stable walking on an uneven floor possible. The experiments of the first phase shows that our humanoid can walk at 1.3km/h and overcome 1cm protrusions successfully.**

I. Introduction

The human-like form of biped humanoids allows these robots to coexist with humans very easily. They can climb up stairs, avoid obstacles on floors, and provide useful service for us, while at the same time presenting a friendly appearance. However, unlike wheel-based service robots, biped humanoid robots have a very complex mechanical structure and are difficult to control. Though the development of ideal companion robots which have human-level motion capability and intelligence is a fantastic goal, it still remains a challenging subject.

Since Waseda University's first humanoid robot in the 1970s[1], many biped humanoid robots have been built in both industry and academia for a variety of purposes. As a pioneer of humanoids in industry, Honda has been using their well-known humanoid, ASIMO[2], mainly for advertisement and publicity campaigns in various event shows. Toyota[3] has also developed biped humanoid robots mainly for exhibition, stating that their future target is the development of partner robots. Sony had produced diverse research outcomes with its entertainment humanoid QRIO[4], until it closed down the project in 2006. Fujitsu sells its small biped humanoid HOAP3[5] as a research platform to universities. Another research humanoid platform HRP-2[6] developed by AIST and Kawada Industries are widely provided to institutes such as INRIA, CNRS, Brussel University, etc., for the study of practical whole body motions. In academia, University of Tokyo[7], Waseda University[8], Technical University of Munich[9], KAIST[10], Beijing University[11], and many others, have developed their own biped humanoid robots for robotic research.

Fig. 1. Biped humanoid robot Mahru III.

Samsung Electronics Co., Ltd. has also developed biped humanoid robots, participating in the Network-based Humanoid Project of the Korean Ministry of Information and Communication (MIC). This project is one of the national robotic research projects of MIC, with the ultimate goal of supplying network-based robots to every household.

The first biped humanoid robot platform we built with KIST was called Mahru II(male) and Ahra II(female). The platform designed and manufactured till November, 2005, showed dancing performance in public, through cooperation with KIST to integrate whole-body motion generation, vision-based manipulation and face detection methods[12]. The name "Mahru" and "Ahra", determined by a survey of public opinion done by MIC, originate from ancient Korean words for "top" and "wisdom" respectively.

This paper's biped humanoid robot Mahru III (Fig. 1), as our second platform, was developed from June 2006 to January 2007, for 7 months. While building this platform, we settled most of the technical problems discovered and listed in the design and experiments of the previous Mahru II and Ahra II platforms.

In this paper, we present the system overview, the design

of mechanical systems and electrical/electronic parts, and the outline of the walking control algorithm. Also, we describe the experimental results of the current phase and future research targets for improved motion performance and network-based applications.

II. System Overview

The kinematic structure of the humanoid Mahru III, composed of 32 joints, is depicted in Fig. 2. The design process of this structure will be given in the following section.

Hardware specifications of the humanoid are described in Table I. The DOF of the hand will be increased from 2 to 8 by the end of 2007 so that the total DOF will increase to 44. Although the mechanism and the actuating systems (motors and harmonic drives) are designed to achieve maximum walking speed at 2.6km/h, which is dramatically higher than that of Mahru II(0.54km/h), current stable walking speed is limited to 1.3km/h due to reasons that will be described later. We expect the target speed of 2.6km/h can be realized, if experiments on the walking control algorithm, as will be discussed in Section V, are completed as planned. The humanoid Mahru III is also able to walk on uneven floors with 1cm protrusions. The operation hour of the Lithium-Polymer batteries mounted on the platform is estimated as 30 minutes. Total weight of the humanoid including exterior appearance parts and batteries is 62kg, which is reduced from the previous Mahru II's 75kg.

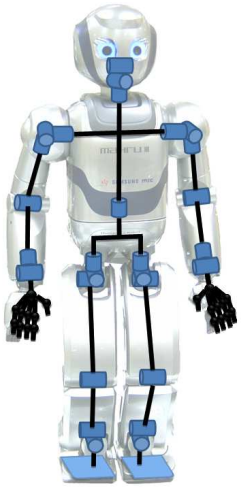

Part	DOF
Head	3
Shoulder	3
Elbow	1
Wrist	2
Hand	2
Waist	1
Hip	3
Knee	1
Ankle	2

Fig. 2. Kinematic Structure of Mahru III

TABLE I
Hardware Specification

Height	150 (cm)
Weight	62 (kg)
Total DOF	32
Maximum walking speed (Current)	1.3 (km/h)
Maximum walking speed (Target)	2.6 (km/h)
Maximum height of bump	1 (cm)
Battery operation hour	30 (min)

In designing the appearance of the face and the body in Fig. 3, smartness, cleverness and human-friendliness are considered as key factors. Moreover, to embody vitality in the face of the humanoid, we added blue blinking LED systems around the eyes and ears.

Fig. 3. Drawing of the face and exterior parts design

III. Mechanical System Design

The key feature of this humanoid, which distinguishes it from others, is that the mechanical system is carefully designed by CAE(Computer Aided Engineering) and DOE(Design of Experiments)-based optimization. The purpose of this optimal design process is the realization of light weight, high stiffness, and high energy efficiency. Toward these goals, kinematic structure is at first designed to minimize load torque guaranteeing large motor speed limits of the lower body, and to maximize manipulability measure of the upper body. Then, CAE analysis and topology optimization for metallic frames are done aiming at light weight and high stiffness of the whole mechanism. Actuating systems are selected to minimize motor power consumptions. This section will introduce such design processes briefly. For further details, please refer to [13].

A. Kinematic Design

When determining the kinematic structure, we considered the similarity to human in terms of shapes, ratios, and physical lengths as important criteria. With these criteria and motion generation capability in mind, we first designed arms and legs to have 6 DOF, waist one DOF, and neck three DOF, respectively. Based on this guideline, detailed position of the joints and length of the links are solved through dynamics simulation and DOE-based optimization as follows[13].

Figure 4 shows (a) the upper body in Denavit-Hartenberg (D-H) representation[14] and (b) the lower body with link lengths of the humanoid. The design parameters to be optimized are b_y, α_b, d_3, a_3, a_4, d_5, and a_6 in Fig. 4(a) and L_0, L_1, L_2, and L_3 in Fig. 4(b). As the objective function of optimization for the upper body, we chose the Manipulability Measure(MM)[14] which indicates the degree of ability to

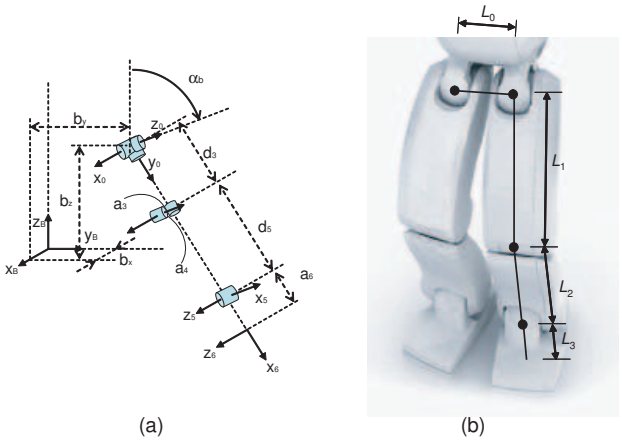

Fig. 4. Parameters for DOE-based optimal kinematic design. (a) D-H parameters of the left arm of the upper body. (b) Link parameters of the lower body.

manipulate objects and is computed as $det(\sqrt{J^T(\theta)J(\theta)})$ where $J(\theta)$ is the Jacobian matrix. We assumed dense grid points, where MM is computed, covering the main workspace of the upper body. Then, by the DOE technique, optimal D-H parameters are obtained to maximize MM at all the grid points. In the case of the lower body, all procedures are the same except that D-H parameters are replaced by link parameters and that load torques and joint speed limits calculated from dynamics simulation are considered as objective functions. Throughout the optimization procedures, the boundary values of the design parameters are given from the human's corresponding average values.

Furthermore, for advanced whole-body motion capability, the movable ranges of the joints are designed to be similar to those of HRP-2 which are the widest amongst known humanoids. Table II shows the comparison results of joint angle ranges of normal human, HRP-2, and our humanoid Mahru III. Although Mahru III does not have a cantilever type structure like HRP-2, elaborate design of the kinematic structure and exterior appearance parts enables Mahru III to have similar joint angle ranges to HRP-2.

B. Frame Design using Topology Optimization and CAE Analysis

After determining the basic kinematic structure, it is required to design the metallic frames which act as the supporting skeleton of the whole body. Shape of the frames should be determined to obtain high stiffness under the constraint of minimizing total weight. We employed topology optimization method to develop stiff and light frames of the lower body for stable walking. Topology optimization is an effective FEM-based technique to design the layout of a body in its initial design step to achieve the above objectives.

Some examples of the topology optimization results are included in Fig. 5. With the exception of fixed area such as joint and motor mounting part in the frame, we applied topology optimization to the remaining area to reduce its mass

TABLE II
COMPARISON OF JOINT ANGLE RANGES

Joint			Human	HRP-2	Mahru III
Head		R	-50° ~ 50°	N/A	-15° ~ 15°
		P	-50° ~ 60°	-30° ~ 45°	-30° ~ 45°
		Y	-70° ~ 70°	-45° ~ 45°	-50° ~ 50°
Right Arm	Shoul-der	P	-180° ~ 50°	-180° ~ 60°	-180° ~ 60°
		R	-90° ~ 0°	-95° ~ 10°	-95° ~ 10°
		Y	-90° ~ 90°	-90° ~ 90°	-90° ~ 90°
	Elbow	R	-145° ~ 0°	-135° ~ 0°	-135° ~ 0°
	Wrist	Y	-90° ~ 90°	-90° ~ 90°	-90° ~ 90°
		R	-70° ~ 90°	-90° ~ 90°	-50° ~ 50°
Waist		P	-30° ~ 45°	-5° ~ 60°	N/A
		Y	-40° ~ 40°	-45° ~ 45°	-50° ~ 50°
Right Leg	Hip	Y	-45° ~ 45°	-45° ~ 30°	-45° ~ 30°
		R	-45° ~ 20°	-35° ~ 20°	-35° ~ 20°
		P	-125° ~ 15°	-125° ~ 42°	-100° ~ 40°
	Knee	P	0° ~ 130°	0° ~ 150°	0° ~ 150°
	Ankle	R	-20° ~ 30°	-20° ~ 35°	-20° ~ 20°
		P	-20° ~ 45°	-75° ~ 42°	-75° ~ 40°

while maximizing the structural stiffness. From the original concept drawing in Fig. 5(a), we obtained first results shown in Fig. 5(b), where blue regions are the area allowed to be removed. Table III demonstrates the effects of topology optimization applied to the lower body frames: each mass is reduced from its original value and accordingly structural stiffness per unit mass increases.

However, leaving the blue region blank may lead to poorer dynamic stiffness of the frame by lowering the resonant frequency. Therefore, we performed CAE-based modal analysis of the frames to determine the minimum thickness of the blue regions. Based on the results, we finally decided shapes and the thickness of the thin area in Fig. 5(c) while additionally considering manufacturing conditions and buckling effects.

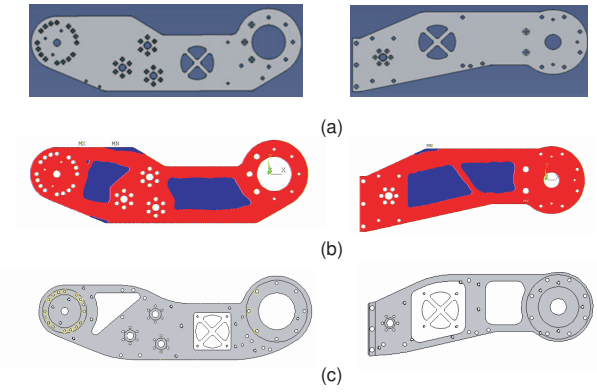

Fig. 5. Designed frames by topology optimization and CAE analysis (a) Original concept (b) Topology optimization results (c) Final frame models

Fortunately, candidate positions of the ventilation holes given from the CAE-based air flow analysis are located within the thin areas. Therefore, we were able to create an effective cooling systems by making the holes and installing cooling fans inside the thin areas as in Fig. 5(c).

TABLE III

RESULTS OF TOPOLOGY OPTIMIZATION OF THE LOWER BODY

	thigh	shin	hip	ankle	waist
Mass reduction ratio	4.2%	5.4%	22.0%	4.0%	46.8%
Increase in stiffness per unit mass	92.2%	129.8%	36.7%	37.0%	90.0%

C. Actuating System Design

Finally, we designed actuating systems by selecting the appropriate harmonic drives and motors with consideration to light weight and high energy efficiency. With the kinematic structure and dynamic model of the designed frames, we conducted walking simulations at various walking speeds to compute load torques and angular speeds at all joints. Figure 6 shows an example of the plot of joint speeds versus joint load torques during walking at 2.6km/h. In addition to walking, other required whole body motions such as sitting and kneeling were also simulated. Then, by overlaying the trajectory on the specification chart offered by manufacturers of motors and harmonic drives, we chose the lightest possible pertinent actuating parts[13]. Consequently, we were able to lighten our humanoid by reducing weights of motors and harmonic drives. Also, we reduced the required power capacity of all motors by 21% from the previous platform.

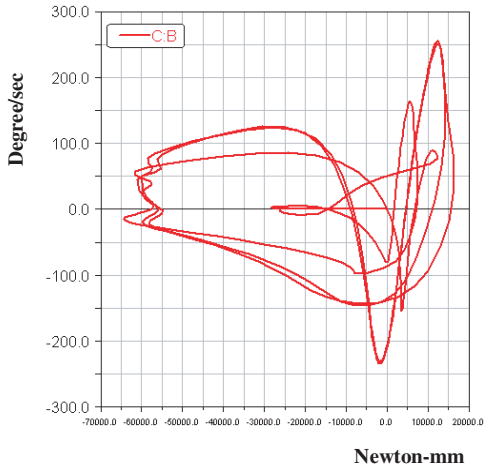

Fig. 6. Knee joint velocity vs torque plot

Meanwhile, we noted that there are stiffness losses in some connecting parts between actuators and frames. To resolve this effect, we used double direction cross roller bearing systems especially on the hip yaw joint. Thus, the clearance of the bearing is significantly reduced and the joint can endure steady load to the bearing system.

IV. ELECTRICAL/ELECTRONIC SYSTEM

Figure 7 is a conceptual diagram briefly describing the electrical and electronic system of Mahru III. It includes CPU boards, local joint control boards and AD converters for motion control; a stereo camera, a pose sensor, and 4 force/torque sensors for sensing; network devices, hub boards, and a communication master board for communication; and batteries and power distribution boards for power regulating.

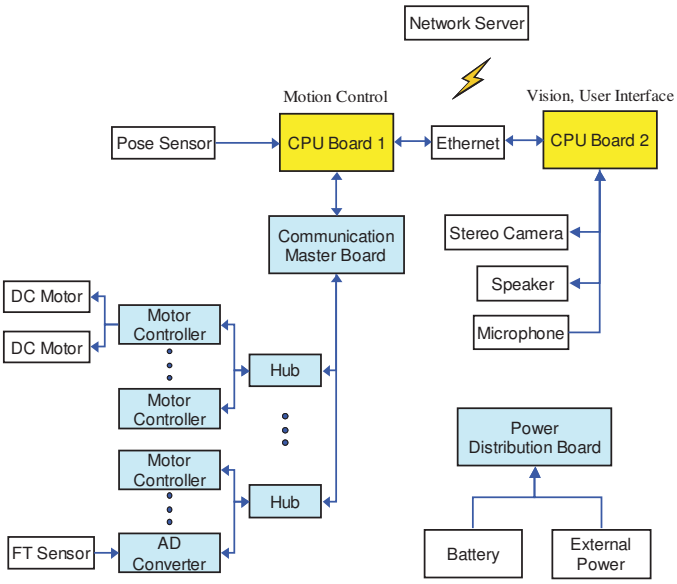

Fig. 7. Electrical/Electronic system of Mahru III

The dual CPU boards structure is employed to deal with future practical network-based applications. In this structure, the processes of the CPU are divided and assigned to each board to reduce computational loads: one is for real-time motion control and the other is for network communication, vision processing, and user interface. It is our long-term goal to make the latter processes be executed by remote servers via "ubiquitous" networks[12]. As the real-time OS, we chose RT-Linux for reliable real-time performance.

To guarantee safe real-time motion control, we decided to use a decentralized control architecture where local control boards have a role of joint servo control, following commands from the main control board. This control architecture has some advantages over a centralized version: 1) since the main board and individual local boards share computations for real-time control, total system is computationally efficient and thus the number of joints to be controlled simultaneously can increase easily, 2) since all joint control run independently, this architecture can prevent local system failures from influencing the whole system.

Some key specifications of the electrial/electronic system are listed in Table IV. As shown in this table, control frequency of the local joint servo control board is ten times of that of the main board. The local board adds 9 interpolation points between consecutive commands from the main board and runs servo control algorithm for each point. The maximum number of available channels of the communication master board is 48 which can cover the required total DOF 44, as mentioned in Section II, plus 4 AD converters for force/torque sensors. We used commercialized communication devices and protocol which guarantee high reliability and 9.3 Mbps data transmission speed. By using hub systems, the total number of

	Double Support Phase	Swing Phase		Double Support Phase	Stance Phase		Double Support Phase
		First Half	Last Half		First Half	Last Half	
z	Predefined Pattern	Predefined Pattern	Impedance Control	Impedance Control	Return to Predefined Pattern	Predefined Pattern	Predefined Pattern
Roll	Hold Modified Orientation	Return to Predefined Pattern	Impedance Control	Impedance Control	Hold Modified Orientation	Hold Modified Orientation	Hold Modified Orientation
Pitch	Hold Modified Orientation	Return to Predefined Pattern	Impedance Control	Impedance Control	Hold Modified Orientation	Hold Modified Orientation	Hold Modified Orientation

Fig. 8. Impedance control modulation according to walking phase

harness lines - power, communication, sensor, etc. - is reduced to 285, which is approximately 70% of the previous platform. We still regard this as large, and continued effort to minimize harness line is being made.

TABLE IV
ELECTRICAL/ELECTRONIC SYSTEM SPECIFICATION

Sampling period at main control	5 (msec)
Sampling period at local control	0.5 (msec)
Maximum number of local control channels	48
Data communication speed	9.3 (Mbps)
Number of harness lines	285
Maximum joint servo tracking error	0.2 (deg)

While the maximum servo tracking error of the local joints during walking was 1.6 degree for the previous platform, current Mahru III has shown only 0.2 degree error, owing mainly to the improvement of the servo control algorithm and mechanical systems. Additionally, we will implement adaptive joint servo control strategy according to walking phase, in order to handle landing impact situations effectively[17], in the future.

V. CONTROL ALGORITHM

This paper's walking control algorithm consists of walking pattern generation, impedance control for landing and uneven surface walking, and real-time ZMP control for reflex control, as shown in Fig. 9.

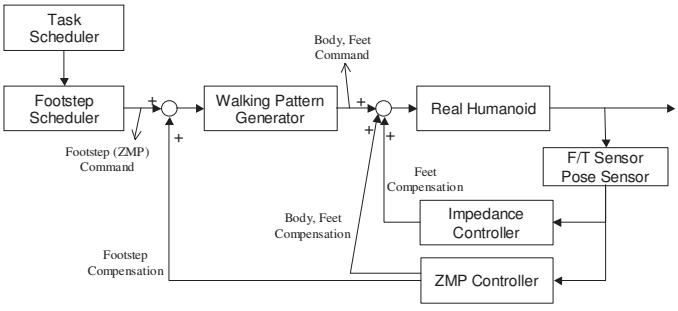

Fig. 9. Concept diagram of walking control algorithm

A. Walking Pattern Generation

In order for a biped humanoid robot to preserve its balance, the ZMP(Zero Moment Point) should be maintained inside of the supporting polygon determined by the supporting feet. We employed the ZMP preview control proposed by Kajita et al.[15] to generate walking patterns which satisfy such constraints on ZMP. Given future ZMP commands, this method provides us with the trajectory command of the body in the inverted pendulum model by using LQ (Linear Quadratic) optimal servo control[16]. This method is simpler than other methods which use trajectory connections obtained from analytic solutions of the ZMP equation[17]. Also, it can deal with arbitrary footsteps more easily. However, only replaying the generated stable walking pattern alone cannot make stable walking possible because of disturbance from unevenness of the floor and landing impacts. Thus, we designed impedance control for landing and will integrate real-time ZMP control for reflex control, as will be shown in the following subsections.

B. Impedance Control for Landing

Impedance control of the leg and ankle has been applied to absorb the impact at foot landing and help maintain balance on uneven surfaces during walking. Conventional impedance control requires the ability to control torque at the joints, which is not easily achieved with the harmonic drives and controller of the current platform. Therefore, for this humanoid platform, a discretized numerical form of impedance control is implemented, using the ankle F/T sensor data. This is similar to the nonlinear compliance control used by Hashimoto et al. [18] and is shown in (1). The impedance control is applied to three directions: the height of the foot (z-direction), the ankle roll and the ankle pitch as

$$\begin{aligned} \Delta z(t) &= \frac{F_z + C_z \Delta z(t-\Delta t)/\Delta t}{K_z + C_z/\Delta t} \\ \Delta\theta_x(t) &= \frac{F_{\theta x} + C_{\theta x} \Delta\theta_x(t-\Delta t)/\Delta t}{K_{\theta x} + C_{\theta x}/\Delta t} \\ \Delta\theta_y(t) &= \frac{F_{\theta y} + C_{\theta y} \Delta\theta_y(t-\Delta t)/\Delta t}{K_{\theta y} + C_{\theta y}/\Delta t} \end{aligned} \quad (1)$$

where Δz, $\Delta\theta_x$ and $\Delta\theta_y$ are the impedance displacement in the foot z-direction, ankle roll direction and ankle pitch direction respectively, and F_z, $F_{\theta x}$ and $F_{\theta y}$ are the force/torque readings from the sensor in the three directions. The equations were derived from the continuous form of a simple impedance system with a spring and damper, as shown in

$$F_i = K_i \Delta_i + C_i \dot{\Delta}_i. \quad (2)$$

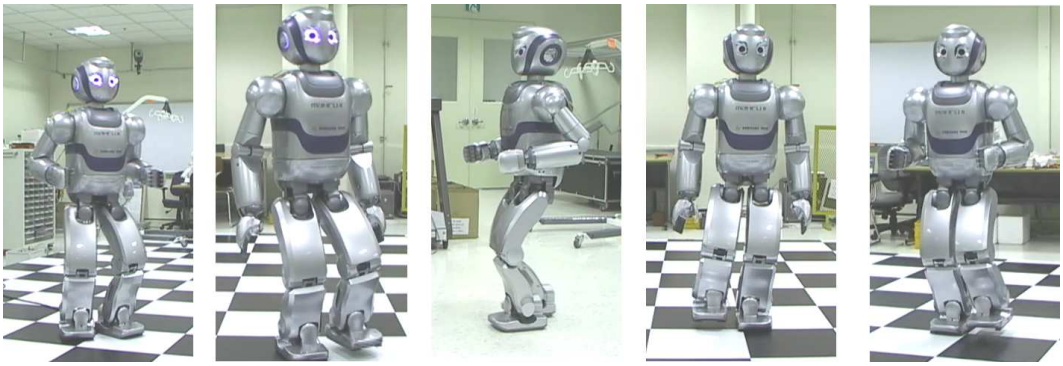

Fig. 10. Various walking experiments

Therefore, K_i and C_i in (1) are the corresponding spring and damping coefficient for each direction. These coefficients were tuned by monitoring ZMP errors during walking trials at various walking speeds and surfaces. Lower spring and damping coefficients were set for higher walking speeds, as a result of the tuning process.

The impedance control is modulated according to the walking phase, as shown is Fig. 8. Impedance control is turned on during the latter half of the swing phase and the double support phase. The displacement in the z-direction is recovered during the single support stance phase whereas the ankle displacements are recovered during the swing phase. A 5-th order polynomial was used to generate the recovery pattern. Holding the ankle displacement during the stance phase resulted in more stable walking.

C. Real-time ZMP Control for Balancing

Similar to Honda[2], AIST[6], and University of Tokyo[17], we propose to use the acceleration of the body to control the ZMP for reflex control. In this control, to reduce the effects of model uncertainty and external disturbance and to increase the stability margin, the LQG(Linear Quadratic Gaussian)/LTR(Loop Transfer Recovery) technique[16] is applied. This robust controller is designed and simulated to compensate for the error from model uncertainty, insufficient stiffness of the mechanism, ground uncertainty, and external disturbance force. However, this algorithm has not been demonstrated in our experiments yet. We will present detailed explanation and experimental results in our next publication.

VI. Experimental Results for Walking and Discussion

The biped humanoid robot Mahru III's walking experiments on a floor of an office are shown in Fig. 10. Stable walking patterns generated from ZMP preview control, and impedance control at ankles were enough to achieve maximum walking speed of 1.3km/h. Moreover, walking on an uneven surface such as a floor with bumps of 1cm height was successful.

However, walking control without ZMP error compensation may be insufficient. This is because such control does not guarantee the ZMP lies inside the supporting polygon when significant external disturbance is exerted or walking speed exceeds a certain value. This is the main reason why the maximum walking speed of Mahru III was limited to 1.3km/h rather than 2.6km/h, which was determined as the target speed when the mechanical system was designed.

Therefore, we plan to combine ZMP control using LQG/LTR technique as explained in the previous section, with the existing walking control 1)to achieve robust walking against external disturbance and 2)to raise the maximum walking speed up to 2.6km/h. Additionally, we will develop whole-body motion control to make practical motions other than pure walking, such as lifting heavy objects, stepping for balancing, reaching for a target object, passing under/over obstacles, and imitating human gesture.

VII. Conclusion

This paper presents the overview of our biped humanoid Mahru III(150cm, 62Kg). The main distinctive characteristics of this humanoid are the optimally designed mechanical system based on CAE techniques and the extensible electrical/electronic system targeting future network-based applications. Light weight, high stiffness, and high energy efficiency of the mechanism are achieved through kinematic design using DOE, frame design based on topology optimization and CAE analysis, and actuating system design through dynamic simulation. Based on this mechanism and the improved decentralized control system, stable walking at 1.3km/h was realized. Furthermore, impedance control modulation according to walking phase allows the humanoid to walk over an uneven floor with 1cm protrusions. As future research topics, we will integrate robust walking control and whole-body motion control to enhance its motion capability. This humanoid will serve as a test platform to perform various motion tasks and examine practical applications incorporated in ubiquitous networks.

Acknowledgment

This work was supported in part by Korean Ministry of Information and Communication(MIC) & IITA through IT Leading R&D Support Project. The authors would like to thank Dr. Ji Oh Song, the former President of our center, for his support for our research. The authors also thank Dr. Bum-Jae You, Dr. Yonghwan Oh, and Dr. ChangHwan Kim at KIST for their technical advice.

REFERENCES

[1] A. Takanishi, M. Ishida, Y. Yamazaki, and I. Kato, "The realization of dynamic walking by the biped walking robot WL-10RD," *Proc. Int. Conf. on Adv. Robotics (ICAR)*, pp.459-466, 1985.

[2] Y. Sakagami, R. Watanabe, C. Aoyama, S. Matsunaga, N. Higaki, and K. Fujimura, "The intelligent ASIMO: System overview and integration, " *Proc. IEEE/RSJ Int. Conf. on Intell. Robots and Systems*, pp.2478-2483, 2002.

[3] http://www.toyota.co.jp/en/special/robot/.

[4] T. Ishida, Y. Kuroki, and J. Yamaguchi, "Mechanical system of a small biped entertainment robot," *Proc. IEEE/RSJ Int. Conf. on Intell. Robots and Systems*, pp.1129-1134, 2003.

[5] R. Zaier and S. Kanda, "Piecewise-linear pattern generator and reflex system for humanoid robots," *Proc. IEEE Int. Conf. Robotics and Automation*, pp.2188-2195, 2007.

[6] K. Kaneko, F. Kanehiro, S. Kajita, H. Hirukawa, T. Kawasaki, M. Hirata, K. Akachi, and T. Isozumi, "Humanoid robot HRP-2," *Proc. IEEE Int. Conf. Robotics and Automation*, pp.1083-1090, 2004.

[7] S. Kagami, K. Nishiwaki, J. Kuffner, Y. Kuniyoshi, M. Inaba, and H. Inoue, "Online 3D vision, motion planning and bipedal locomotion control coupling system of humanoid robot: H7," *Proc. IEEE/RSJ Int. Conf. on Intelli. Robots and Systems*, pp.2557-2562, 2002.

[8] Y. Ogura, H. Aikawa, K. Shimomura, H. Kondo, A. Morishima, H. Lim, and A. Takanishi, "Development of a new humanoid robot WABIAN-2," *Proc. IEEE Int. Conf. Robotics and Automation*, pp.76-81, 2006.

[9] S. Lohmeier, K. Löffler, M. Gienger, H. Ulbrich, and F. Pfeiffer, "Computer system and control of biped "Johnnie"," *Proc. IEEE Int. Conf. Robotics and Automation*, pp.4222-4227, 2004.

[10] I. Park, J. Kim, J Lee, and J. Oh, "Mechanical design of humanoid robot platform KHR-3 (KAIST humanoid robot - 3: HUBO)," *Proc. IEEE-RAS Int. Conf. on Humanoid Robots*, pp.321-326, 2005.

[11] Q. Huang, Z. Peng, W. Zhang, L. Zhang, and K. Li, "Design of humanoid complicated dynamic motion based on human motion capture," *Proc. IEEE/RSJ Int. Conf. on Intelli. Robots and Systems*, pp.3536-3541, 2005.

[12] B. You, Y. Choi, M. Jeong, D. Kim, Y. Oh, C. Kim, J. Cho, M. Park, S. Oh, "Network-based humanoids 'Mahru' and 'Ahra'," *Proc. Int. Conf. on Ubi. Robots and Ambient Intelli.*, pp.376-379, 2005.

[13] W. Kwon, J. Park, H. Kim, C. Roh, J. Lee, J. Park, W. Kim, and K. Roh, "An optimal mechanism design method for biped humanoid robots," *Proc. Samsung Tech. Conf.*, 2006.

[14] J. Craig, *Introduction to Robotics - Mechanics and Control*, 2nd edition, Addison-Wesley, 1989.

[15] S. Kajita, F. Kanehiro, K. Kaneko, K. Fujiwara, K. Harada, K. Yokoi, and H. Hirukawa, "Biped walking pattern generation by using preview control of Zero-Moment Point," *Proc. IEEE Int. Conf. Robotics and Automation*, pp.1620-1626, 2003.

[16] B. Anderson, J. Moore, *Optimal Control: Linear Quadratic Methods*, Prentice-Hall, Inc., 1989.

[17] M. Inaba, S. Kagami, and K. Nishiwaki, *Robot Anatomy*, Iwanami Lecture Series 7 on Robotics, 2005 (*in Japanese*).

[18] K. Hashimoto, Y. Suguhara, H. Sunazuka, C. Tanaka, A. Ohta, M. Kawase, H. Lim, and A. Takanishi, "Biped landing pattern modification method with nonlinear compliance control," *Proc. IEEE Int. Conf. Robotics and Automation*, pp.1213-1218, 2006.